

The formation of a cavity in water: changes of water distribution and prediction of the excess chemical potential of a hard-sphere solute under increasing pressure

Franca Maria Floris¹

*Dipartimento di Chimica e Chimica Industriale, Università di Pisa,
Via Giuseppe Moruzzi 13, 56124 Pisa, Italy*

Abstract

This work deals with the formation of a spherical cavity in water along the isotherm at 298 K. A striking effect of increasing pressure was found on the radial distribution functions obtained by Monte Carlo simulations, with significant different behaviours observed when increasing the cavity radius at 8000 atm and 1 atm. Particular focus is on the value at contact, $G(r)$, the central quantity in Scaled Particle Theory that is related to the derivative with respect to the radius of the work required to form the cavity. Within the limit of very small radii, exact conditions were applied to these two quantities. This allowed us to readily determine, at any pressure along the isotherm, the parameters of a simple model used to compute the excess chemical potential associated with the hydration of a hard sphere. This was made possible thanks to heuristic models used to describe how the number density of water changes along the isotherm and how the second moment of water distribution depends on the first moment. Use was also made of additional information on a cavity of molecular size. Apart from the dependence on pressure of hydrophobic solvation, this work also concerns calculation of the so-called cavitation contribution to the free energy of solvation when this is computed within implicit solvent models.

Email address: floris@dcci.unipi.it (Franca Maria Floris)

Keywords: cavity, SPT, simulations, pressure, hydration, distribution moments

1. Introduction

According to thermodynamics [1, 2], excess chemical potential or pseudochemical potential [1] expresses how the free energy of the system changes as a solute molecule is added to the solvent at a fixed position. For a hard-sphere solute-solvent potential, at constant T, this quantity is equal to the reversible work necessary to form a cavity in the solvent [3, 4, 5, 6]. The translation kinetic energy of the solute is added to obtain the chemical potential, from which other important thermodynamic quantities can be computed from derivatives with respect to state variables, such as pressure and temperature [1, 2].

This work studies the pressure dependence of the excess chemical potential associated with the insertion of hard-sphere solutes at infinite dilution in water along the isotherm of 298 K. A purely repulsive potential can be used to model interactions between a hydrophobic solute and water. However, it is also important for the computation of the so-called "cavitation contribution" to the free energy of solvation within polarizable continuum models [7, 5] as the solute is enclosed in a molecular cavity defined by the union of spheres. When using these methods the focus is on the quantum treatment of the solute, and most of the computational time is spent for the electrostatic contribution [8], and, depending on the method used, for the dispersion contribution. [9]. It is in this context that it is useful to develop simple heuristic expressions in order to compute thermodynamic quantities related to the solvation process of these simple modeled solutes [5, 10]. At infinite dilution conditions, interactions between solute molecules can be ne-

23 glected and only solute-solvent interactions give a contribution to the excess chem-
24 ical potential. This can be computed using a coupling parameter method [11],
25 which requires information on how the solvent distribution function changes from
26 the initial state of pure solvent to the final state in which the solute-solvent interac-
27 tion is completely coupled. This method implies the study of "intermediate states"
28 which are generally unrealistic. When applied to a hard-sphere solute-solvent in-
29 teraction, the solute insertion process is equivalent to scaling the radius of a cavity
30 from zero up to a final contact radius, r , as shown in the original paper of Scaled
31 Particle Theory (SPT) [3]. Thus, our interest in the formation of a cavity in a
32 solvent is extended to such small cavities that they cannot host any real solute.
33 Within SPT [3, 4, 6], the excess chemical potential associated with cavity forma-
34 tion is related to the probability that no centers of the solvent molecules will be
35 found in the spherical region defined by the contact radius. On the basis of statisti-
36 cal mechanics, this probability is expressed in terms of pure solvent quantities that
37 can be computed from the number density and integrals involving many-particle
38 correlation functions. These integrals define the second and higher moments of
39 the pure solvent distribution functions and can be written in terms of probabilities
40 that exactly n centers of the solvent molecules can be found in the cavity volume
41 [3]. As specified in the literature [3, 12], the excess chemical potential written
42 in terms of moments is of general validity and can be applied to cavities of an
43 arbitrary shape and using a realistic model potential for interactions between sol-
44 vent molecules. However, as only the first two moments are easily available, its
45 application is limited to very small cavities so that $n \leq 2$ or requires the com-
46 putation of modeled probabilities. These can be computed within an information

47 theory based on the first two moments, as demonstrated by Hummer et. al. [12].
48 Here, we work within SPT and apply the exact relation only to such a small sized-
49 cavity that the excess chemical potential is directly computed from the first two
50 moments. Exact SPT conditions are then applied at an appropriate radius close to
51 the extreme of the range where the contribution of higher moments vanish. These
52 conditions involve derivatives of the excess chemical potential with respect to the
53 cavity radius. In order to facilitate these calculations and apply SPT along the
54 isotherm we describe the two first moments of water for spherical volumes as a
55 function of radius and pressure. Such descriptions make use of a simple relation
56 between the first moment and the water number density [12], which was modeled
57 along the isotherm. This was also used in a heuristic expression proposed here
58 to compute the second moment from the first moment using a modified Poisson
59 distribution (see Appendix A).

60 Scaling the radius from small to larger sized-cavities so that a real solute can be
61 hosted in, the approximate SPT expression [13, 14] or the more flexible expres-
62 sions based on the thermodynamics of surfaces [15] are generally used [16, 5, 10].
63 The effect of pressure on parameters entering such expressions has been little ex-
64 plored until now. At fixed conditions of P and T, such parameters are preferably
65 determined by fitting procedures. However, a complete study of the effect of pres-
66 sure on the thermodynamics of cavity formation would require a great number of
67 very expensive simulations.

68 Here, we test these simple models at a very high pressure by comparison with
69 simulation results. We show that a less expensive parametrization based on exact
70 relations gives results which are in agreement with those obtained by fitting. This

71 was made possible by the use of a relatively simple scheme formulated within the
72 framework of SPT, with a limited number of conditions on the central function
73 $G(r)$, which is defined by the contact value of the cavity-solvent radial distribution
74 function (rdf). As noticed above, these conditions were applied within the limit
75 of a very small cavity, but some information on a molecular-sized cavity was em-
76 ployed in the parametrization. Differently from the approximate SPT expression,
77 this is in fact necessary when using more flexible simple models.

78 2. Calculation

79 2.1. Excess chemical potential and $G(r)$

80 According to statistical mechanics [3], the excess chemical potential of a hard-
81 sphere solute, here denoted by μ^* , can be computed from the probability that an
82 empty region can be found in the solvent and it is written in terms of moments of
83 the solvent distribution. Within the limit of a very small cavity, this exact relation
84 involves only the first two moments,

$$\mu^* = -k_B T \ln \left[1 - \langle n \rangle + \frac{1}{2} \langle n(n-1) \rangle \right] \quad (1)$$

85 where n is the instantaneous number of molecular centers in the pure solvent
86 contained in a sphere of radius r , whose average $\langle n \rangle$ can be obtained from
87 the number density ρ [12]. The third term in brackets gives the average number
88 of pairs in the same volume and can be obtained from integrals involving the pair
89 distribution function [3, 12]. The expression above is valid for cavity volumes
90 for which the contribution of higher moments vanish ($n \leq 2$).

91 For larger cavities, the excess chemical potential is computed with a simple model
92 formulated within the thermodynamics of surfaces [15]. We adopt the most com-

93 mon division [4, 17] related to a cavity of radius r , which here defines the ac-
 94 cessible surface and the exclusion volume to oxygen nuclei positions of water
 95 molecules. Namely,

$$\mu^*(r) = 4\pi\tilde{\gamma}f_c(r)r^2 + P\left(\frac{4\pi}{3}r^3\right) \quad (2)$$

96 where $\tilde{\gamma}$ has the dimension of a surface tension and $f_c(r)$ is a function describing
 97 curvature corrections, which equals 1 for a cavity in the limit of an infinite radius.
 98 The average density of solvent centers on the cavity surface is given by $\rho G(r)$,
 99 and $G(r)$ is related to μ^* by the important relation derived from SPT [3, 16],

$$G(r) = \frac{1}{4\pi r^2 \rho k_B T} \frac{d\mu^*}{dr}. \quad (3)$$

100 As remarked by Reiss et al. [3], μ^* equals the reversible work which is expended
 101 in the formation of the cavity. Given that this process is equivalent to the coupling
 102 of a hard-sphere interaction potential with contact distance r , the value of the
 103 rdf for the solvent centers excluded from the spherical region coincides at r with
 104 $G(r)$. Thus, as pair correlation functions are commonly calculated in simulations,
 105 this relation is very useful to validate simple models used to describe the radial
 106 dependence of f_c in Eq. (2). The general form of this model leads to the following
 107 simple expression for the derivative of μ^* with respect to r ,

$$\frac{d\mu^*}{dr} = 4\pi\tilde{\gamma} \left(2r - 2\tilde{\delta} + \frac{\alpha}{r^2} \right) + P(4\pi r^2) \quad (4)$$

108 where $\tilde{\delta}$ and α are parameters entering the curvature correction $f_c(r)$ [16, 10].

109 *2.2. Solvent Compressibility*

110 **The** coefficient of isothermal compressibility can be derived from density in ac-
111 cordance with the thermodynamic definition:

$$k_T^\circ = -\frac{1}{V} \left(\frac{\partial V}{\partial P} \right)_T = \frac{1}{\rho} \left(\frac{\partial \rho}{\partial P} \right)_T \quad (5)$$

112 **or from volume fluctuations in the NPT ensemble, namely,**

$$k_T^\circ = -\frac{\langle V^2 \rangle_N - \langle V \rangle_N^2}{k_B T \langle V \rangle_N}. \quad (6)$$

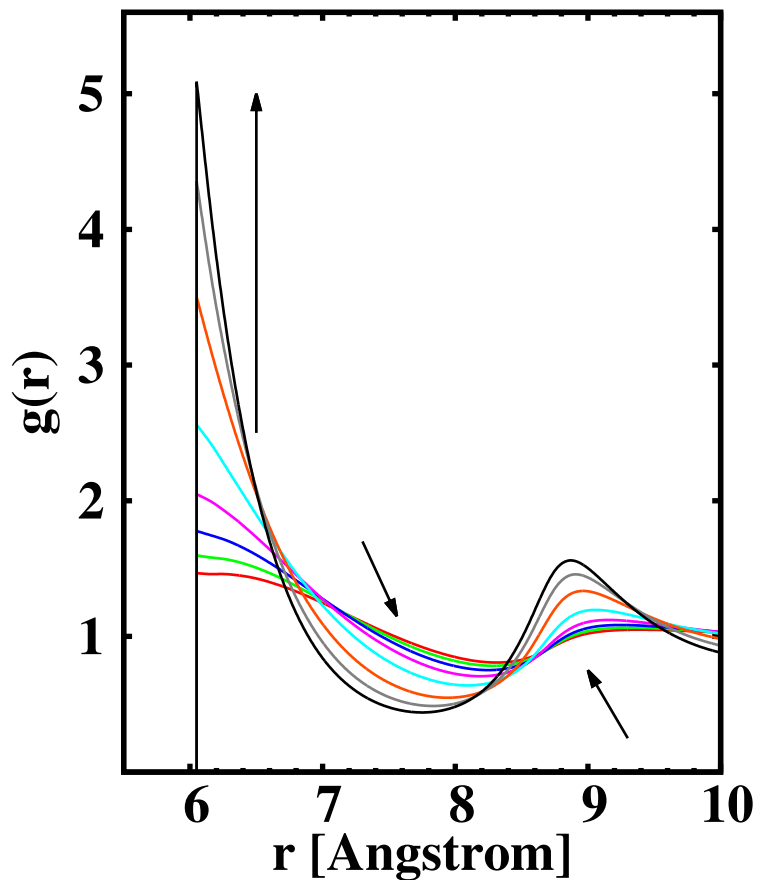
113 **3. RESULTS AND DISCUSSION**

114 *3.1. Simulation Results*

115 NPT Monte Carlo (MC) simulations were run for hard-sphere cavities in 512
116 TIP4P [18] waters for contact radii up to about 6 Å. **This was made by excluding**
117 **the corresponding spherical volume to the motion of water-oxygen nuclei [19, 20].**

118 Cavities in water at ambient conditions have been widely studied in our previous
119 works [21, 10] and by other authors [4, 16, 6]. Since in this work these systems
120 are used as representative of the low pressure limit, we briefly recall the main re-
121 sults. Concerning water distribution, for a cavity radius larger than approximately
122 the most probable distance between the oxygen center with a methane-like so-
123 lute, $G(r)$ rapidly decreases, determining dewetting for nanometric cavities. At
124 the same time, oscillations in the rdf present less pronounced deviations from 1,
125 and cavity water correlations for similar r start to give positive contributions to
126 the excess volume [21]. Fig. 1 shows an example of the **striking** effect of increas-
127 ing pressure on the cavity center-O rdf. In addition to the increased rdf contact

Figure 1: Radial distribution functions vs r , the distance of the oxygen from the center of the cavity with contact radii of 6.05 \AA , at $T = 298.15 \text{ K}$ and P from 1 to 8000 atm. Arrows indicate the direction of increasing pressure.



128 values with respect to those at 1 atm, at 8000 atm (Fig. 2) there is a remarkable
 129 difference regarding the persisting structure when increasing the cavity radius. In
 130 the range $4 - 6 \text{ \AA}$ there is very little increase in the rdf contact value, and at the
 131 extreme of the range this is very close to the asymptotic limit at a large cavity
 132 radius ($P/(\rho K_B T)$).

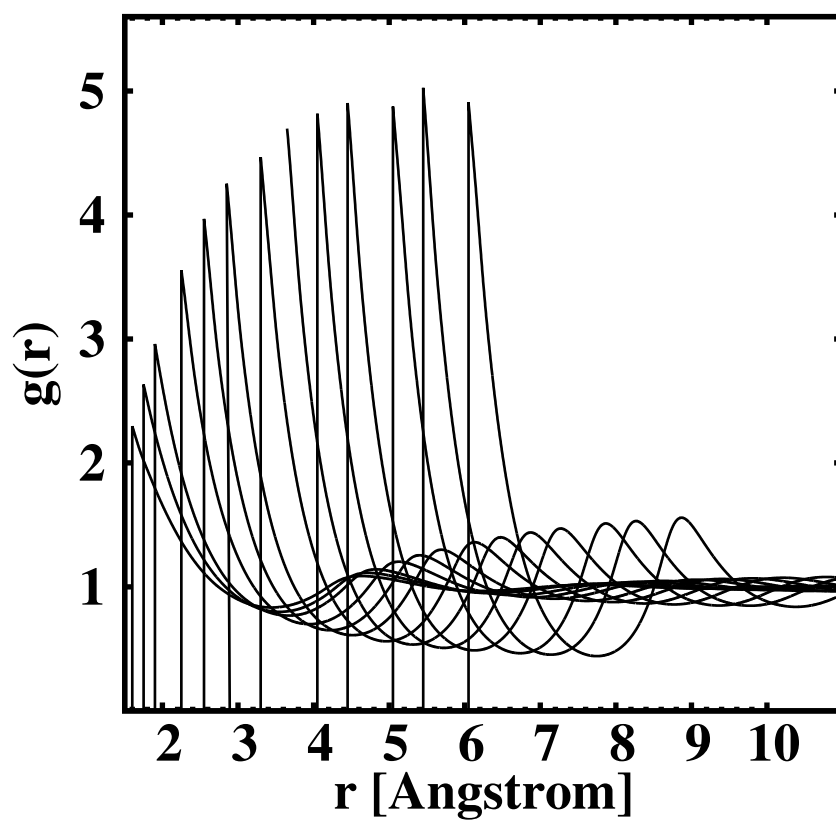


Figure 2: Cavity-water oxygen radial distribution functions for contact radii of 1.60, 1.75, 1.90, 2.25, 2.55, 2.85, 3.3, 3.65, 4.05, 4.45, 5.05, 5.45 and 6.05 Å, at $T = 298.15$ K and $P=8000$ atm. Results from NPT MC simulations of a cavity in 512 TIP4P waters using a modified version of the BOSS program[19].

133 In order to compute μ^* and $G(r)$ from pure solvent quantities, NPT MC simula-
134 tions of 512 TIP4P waters at $T=298$ K and several pressures between 1 atm and
135 10000 atm were run. The O-O rdfs are shown in Fig. 3, while the density and
136 compressibility results are reported in Table 1. These are in good agreement
137 with simulation results obtained with the same model [22, 23], but with a fewer
138 number of water molecules (216 and 365). The comparison made in Fig. 4 with
139 experimental data is in line with what has already been observed in the literature
140 [22]. The same can be said about the comparison with simulation results with the
141 TIP5P model [24].
142 Furthermore, expressions proposed in this work to describe the pressure depen-
143 dence of density and the related quantities entering the exact relation (Eq. 1) of
144 μ^* used for small cavities are validated by comparison with simulation results for
145 radii of 1.6 Å, 1.75 Å and 1.90 Å. This validation is important in the parametriza-
146 tion of the μ^* expression used for larger cavities (Eq. 2). In order to establish how
147 the surface tension parameter depends on pressure, additional information on a
148 larger cavity is necessary. To this end, $G(r)$ values were used from simulation
149 results at various P along the isotherm, for a cavity radius of 6.05 Å. It can be
150 noticed that this radius is small enough for the box size used so that systematic er-
151 rors were avoided. Nevertheless, it is larger than the radius of a cavity appropriate
152 to host a fullerene molecule. Since the rapid convergence of $G(r)$ values observed
153 when increasing the radius at 8000 atm and on the basis of the behaviour ob-
154 served at ambient conditions, we think that, the procedure implemented to test
155 simple models would give comparable results with fitting to data in a range up to
156 approximately 10 Å.

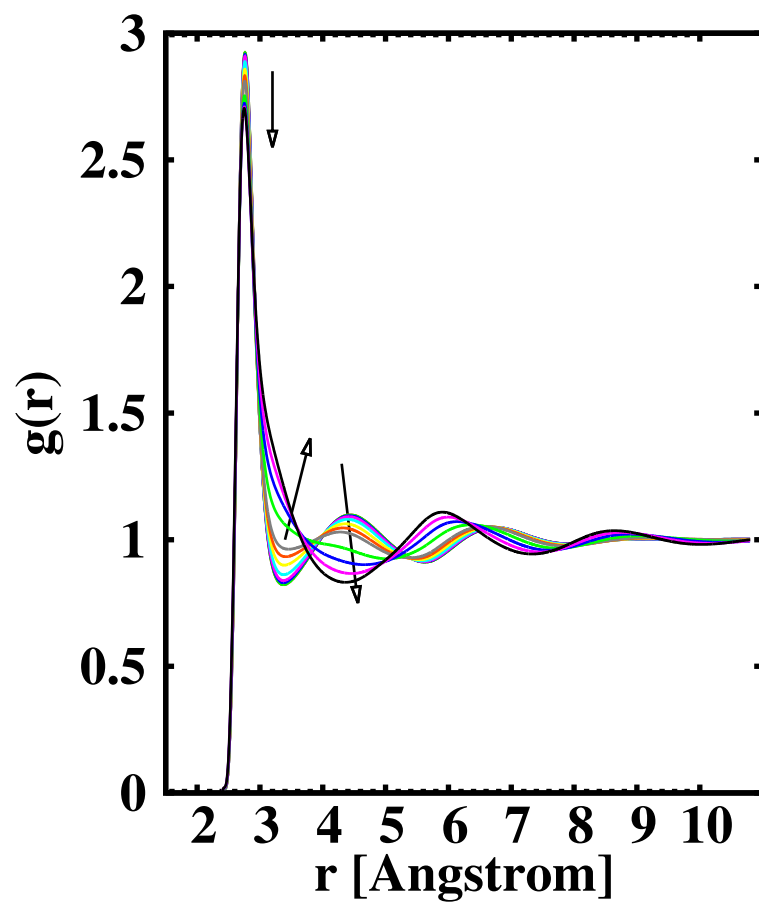


Figure 3: O-O radial distribution function for 512 TIP4P waters at T=298 K and P between 1 atm and 10000 atm. Arrows indicate the direction of increasing pressure.

Table 1: NPT MC results for the density and the coefficient of isothermal compressibility obtained for 512 TIP4P waters at 298.15 K and various P. The numbers in parentheses are the statistical uncertainties in the last digit.

P (atm)	ρ (g/cm ³)	$10^6 k_T^\circ$ (atm ⁻¹)
1	0.99754(2)	51.93(1)
100	1.00276(5)	50.57(3)
200	1.00779(5)	44.84(6)
500	1.02294(5)	45.25(3)
1000	1.04587(4)	40.11(2)
1500	1.06675(5)	35.96(2)
2000	1.08560(5)	32.56(2)
4000	1.14779(6)	22.80(2)
6000	1.19479(6)	18.30(7)
8000	1.2349(2)	14.50(2)
10000	1.26846(6)	12.05(1)

157 *3.2. P dependence of water density and compressibility*

158 **In this section we present models to describe how the water number density, ρ ,**
 159 **changes along the isotherm at T 298 K.** In agreement with the observed P de-
 160 pendence of the average volume of a fixed number of water molecules **a good**
 161 **description was obtained** by the following expression:

$$\frac{1}{\rho(P)} = t_0 + t_1 P + t_2 P^2 \ln(P/P_0) + t_3 P^{2.5} + t_4 P^3 \quad (7)$$

162 where P_0 is the unity used for pressure, here 1 atm, t_0 , t_1 , t_2 , t_3 and t_4 are con-
 163 stant parameters. As shown in Fig. 4, this equation performs very well in fitting
 164 TIP4P simulation results as well as experimental data [25] (see Supporting Infor-
 165 mation(SI) for parameters). **Less satisfactory fitting was instead found with the**

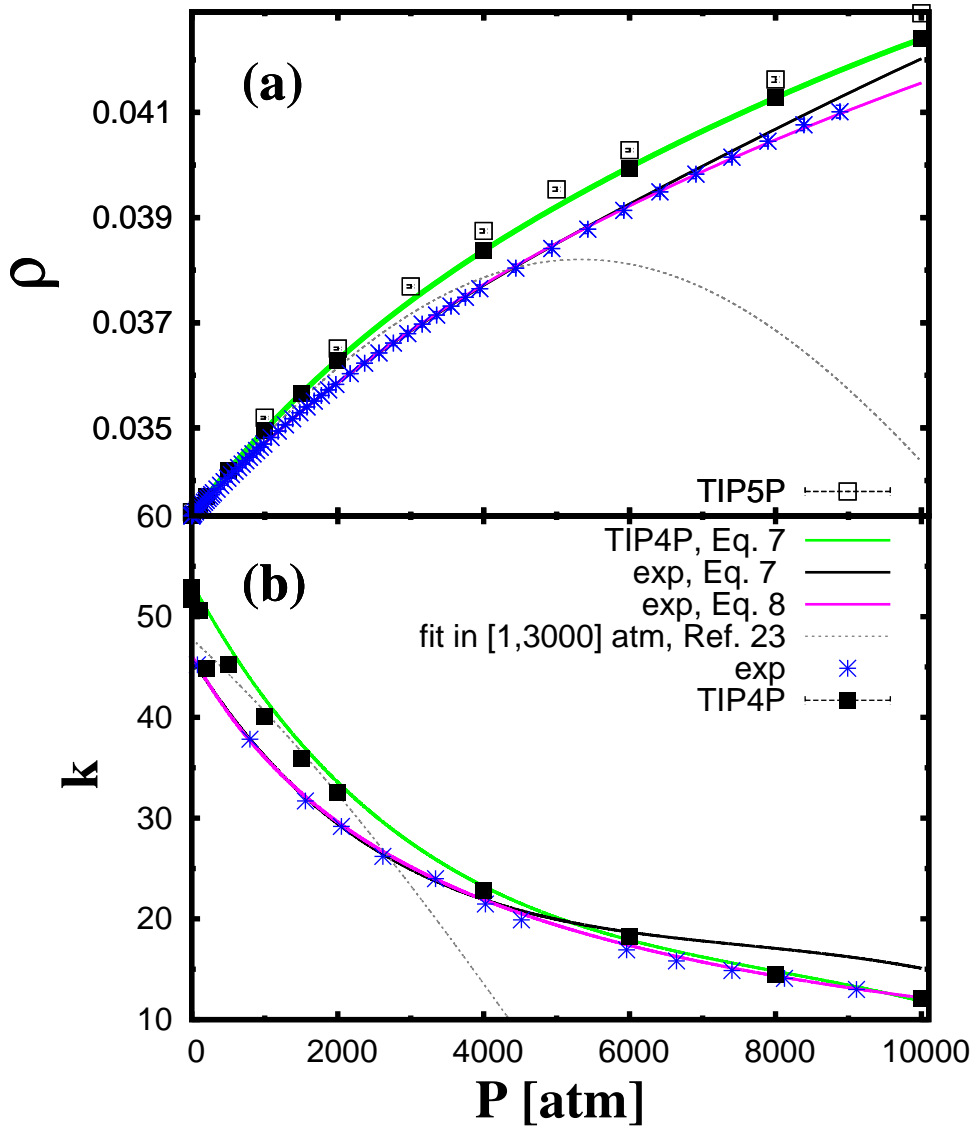


Figure 4: Pressure dependence of the water number density (a) and the isothermal compressibility (b) at $T = 298.15$ K. Simulation results of this work computed for boxes of 512 TIP4P waters are indicated by filled squares (for statistical uncertainties and units see Table 2). Comparison is shown with other simulation results (empty squares) obtained for boxes of 512 TIP5P waters [24], and with experimental results (stars). Lines indicate results obtained using least-square fits to simulation and experimental data of the number density with Eqs. 7 and 8 from which the corresponding isothermal compressibility was obtained using Eq.5. Short dashed lines refer to literature data [23] obtained from the quadratic fit of $\langle V \rangle$ of 365 TIP4P waters.

166 semi-empirical Tait equation and even the modified Tait equation [26]. Instead,
167 a quadratic fit of the average volume was found acceptable only in a limited pres-
168 sure range up to approximately 3000 atm. This simple model has been used in this
169 range to fit data of a smaller box of TIP4P waters [23]. The curve is reported in
170 the figure and clearly shows disagreement with our data for pressure greater than
171 3000 atm.

172 In describing the density dependence on pressure, a stringent test on the validity of
173 models is provided by the examination of their performances on isothermal com-
174 pressibility, which is related to the pressure derivative of the density by Eq. (5).
175 As shown in Fig. 4 (b), Eq. (7) is able to predict generally quite well both simu-
176 lation and experimental data. However, systematic errors shown at P greater than
177 6000 atm when fitting experimental data suggest that in this range results obtained
178 with this equation should be interpreted with caution. Thus, to improve compress-
179 ibility results, an alternative expression was also considered. The quantity $-k_T^o V$
180 obtained from the simulation results gives an estimate of the slope of the volume
181 curve plotted against P. The fitting of this curve suggested the following equation
182 for P dependence of density

$$\frac{1}{\rho(P)} = \frac{1}{\rho_0} + \frac{(ab - c)\ln(bP + 1) + bcP}{b^2}. \quad (8)$$

183 (See Supporting Information(SI) for parameters a, b, c). This equation can be seen
184 as a modified Tait equation and gives good density fitting with improved slope at
185 higher pressures when comparison is made with experimental data. However,
186 on simulation results, no significant improvement with respect to Eq. (7) was
187 observed and in this case we show in the figure only the curves that fit TIP4P data

188 with this equation.

189 3.3. Small cavities ($n \leq 2$): P dependence of μ^* and $G(r)$

190 Here we show results obtained from the exact relation written in terms of the
191 first two moments, which is valid for small cavities with a radius so that no more
192 than two centers of the solvent can be found in the spherical volume. At each
193 value of P over the range from 1 to 10000 atm, the average number of oxygen
194 pairs in a specific spherical region was computed by numerical integration of the
195 O-O rdf in pure water (see Fig. 3). Once this quantity was obtained, μ^* and
196 $G(r)$ were computed using the exact relations, Eq. (1) and Eq. (3) respectively
197 [10]. As expected, the cost of cavity formation increases as the pressure increases
198 when radii are sufficiently large, while for cavity radii less than 0.6 Å there is no
199 significant effect of the pressure (see Fig. 5(a)). Namely, with the "radius" of a
200 water molecule of around 1.35 Å, these cavities are inappropriate to host a real
201 solute. Following Reiss et al., in this case, one can think that a point solute has
202 been added to the solvent. However, when excluding a volume to the motion of
203 solvent centers it is not always necessary to associate this with the addition of a
204 solute molecule. These small cavities show, nonetheless, a significant effect of
205 increasing pressure.

206 In the examined range, $G(r)$ increases with the radius with larger slopes at greater
207 P . As shown in Fig. 5(b), comparison with values directly computed by simula-
208 tions at 1 atm and 8000 atm is good. The sudden drop in the curves indicates
209 the failure of Eq. (1) for larger cavity radii so that $n > 2$ [4]. This equation is
210 valid up to a radius that slightly decreases as the pressure increases, passing from
211 1.83 Å at 1 atm to 1.77 Å at 10000 atm. At a first glance, this decrease appears

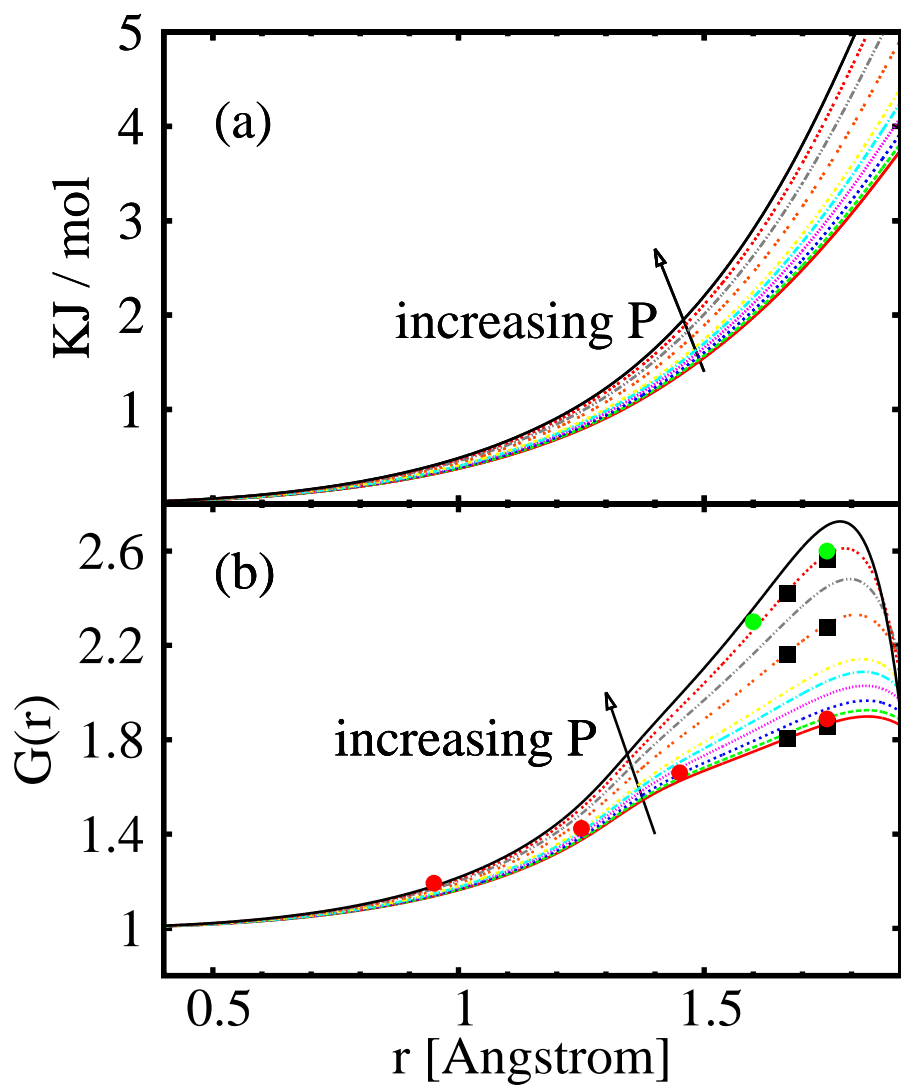


Figure 5: Small cavities ($n \leq 2$) at $T=298$ K. Pressure effect on the radial dependence of (a) μ^* (Eq. (1)) and $G(r)$ (b) (Eq. (3)) over the range from 1 to 10000 atm. In Eq. (1) $\langle n \rangle$ and $\langle n(n-1) \rangle$ were obtained from simulation results of ρ and O-O rdfs (Fig. 3) [3, 4, 10]. Filled squares represent $G(r)$ results from the same equations but with $\langle n \rangle$ and $\langle n(n-1) \rangle$ from Eq. (7) and Eq. (9). $G(r)$ values from the contact values of the cavity-water oxygen rdfs computed by MC simulations of cavities in TIP4P waters are also shown for some radii at 1 atm (filled red circles) and at 8000 atm (filled green circles).

212 to be related to the slight decrease in the most probable O-O distance observed
 213 at greater P (Fig. 3). However, **it certainly arises from** the increased number of
 214 oxygen pairs obtained by integration of O-O rdf in a range of distances up to twice
 215 the cavity radius (see Eq. (5) of Ref. [10]). In this regard, we can notice **that rdf**
 216 **values increase with an increase of pressure at distances of the first peak tail and**
 217 **around the first minimum.** As a consequence, the probability of occurrence of
 218 oxygen triplets in a sphere of fixed radius increases with P, so determining **the**
 219 **observed smaller range of applicability for Eq. (1).**

220 For a cavity of radius r , a quadratic fit of μ^* against pressure can be used. Alter-
 221 natively, using the exact **relation written in terms of the first two moments,** it is
 222 possible to exploit the well established dependence on pressure of ρ (see Section
 223 3.2). To follow this route it is convenient to describe indirectly the P dependence
 224 of the average number of oxygen pairs observed in a spherical region by its de-
 225 pendence on $\langle n \rangle$. It was found that the natural logarithm of this quantity can
 226 be expressed as

$$\log\left[\frac{\langle n(n-1) \rangle}{2}\right] = B \times \left[\log\left(\frac{\langle n \rangle^2}{2}\right) - \langle n \rangle\right] \quad (9)$$

227 where

$$\langle n \rangle = \frac{4}{3}\pi r^3 \rho(P) \quad (10)$$

228 and the factor B is a function of the cavity radius and of $\langle n \rangle (P)$ as detailed
 229 in Appendix A, where a justification of Eq. (9) is given [27]. **We recall that we**
 230 **apply Eq. (9) to small radii such that no more than two water-oxygen centers can**
 231 **occur inside the spherical volume. In this case $\langle n(n-1) \rangle / 2$ is equal to the**

232 probability that exactly 2 centers can be found in this volume [3]. Therefore, this
233 equation is consistent with the probability expression found within information
234 theory when a Poisson default model is used (see for example Hummer et al.
235 [12]). However, in the present work, differently from solutions coming from this
236 theory, the B factor is sought as function of $\langle n \rangle$ instead of n . This implies that
237 parameters are here independent of $\langle n \rangle$. We notice that the form proposed
238 to describe how factor B depends on r and $\langle n \rangle$ correctly gives a number of
239 pairs equal to zero when $\langle n \rangle$ goes to zero and fits the data very well ($n \leq 2$).
240 Hence, using ρ from Eq. (7) in Eq. (10) and introducing $\langle n \rangle$ in Eq. (9),
241 μ^* can be computed from the first two moments by Eq. (1) and, in this manner,
242 its derivatives with respect to r and P can be readily evaluated along the isotherm.
243 In particular, the first and second derivatives with respect to r were computed at
244 any P to obtain $G(r)$ and $G'(r)$. Comparison with results obtained using $\langle n \rangle$
245 and $\langle n(n-1) \rangle$ (via O-O rdfs integrals) from simulations is very good over the
246 range of pressures investigated. For simplicity, in Fig. 5 (b) comparison of $G(r)$ is
247 shown for some selected values of P .

248 *3.4. Parametrization of the approximate SPT expression and simple models*

249 In this section, the approximate SPT expression and simple models derived from
250 the thermodynamic of surfaces [15] are used to estimate μ^* and $G(r)$ for cavity
251 radii larger than 1.7 Å. As already cited in the literature [28, 5, 10, 6, 29], similarly
252 to these simple models, the approximate SPT expression can be written as the
253 sum of a surface and volume terms. Nevertheless, a fundamental distinction
254 between them concerns the limiting radius where they have been formulated,
255 this being subnanometric for the approximate SPT and macroscopic for simple

256 **models.** Such a distinction is important because the number of independent
257 parameters is different and these correspond to different quantities related to one
258 other. This implies that, despite their similarities, these expressions can present
259 different problems **when parametrized at very high pressure.**

260

261 *3.4.1. Approximate SPT: the change of a_w with increasing P*

262 The simplest and most commonly used SPT expression needs only **the solvent**
263 **number density and** the definition of the size parameter of the solvent molecule
264 (a_w), **which can be identified with its hard-sphere diameter.** Inadequacies of this
265 expression are well known from studies at ambient pressure [16, 5, 21, 10], but
266 undoubtedly it is very attractive due to its simplicity. As a first approach, **for wa-**
267 **ter solvent, this parameter** could be fixed at the distance corresponding to the first
268 maximum of O-O rdf (Fig. 3). This is very slightly influenced by P , changing by
269 only 0.01 Å in passing from ambient pressure to 10000 atm. At ambient condi-
270 tions, its value is 2.76 Å which is very close to the value proposed **for a_w** in the
271 earlier work of Pierotti [13]. However, the comparison with **simulation results of**
272 **μ^* and $G(r)$** for hard-sphere solutes in TIP4P water has suggested that the optimal
273 value for this parameter is around 2.9 Å [5, 10].

274 On the basis of the above, only a slight dependence on P is predictable for this
275 parameter in the case that it is assumed to be related to the most probable O-O
276 distance. **Hence, once the functions $a_w(P)$ and $\rho(P)$ are established,** the approx-
277 imate SPT expression can be used to obtain an estimate of the surface tension
278 parameter [28, 5, 29]. With the assumptions made above, $\tilde{\gamma}$ would increase with
279 increasing P because of the dominant effect of increasing density. Is this correct?

280 In order to answer this question, we compare the $G(r)$ values calculated at 8000
281 atm using the approximate SPT expression with those obtained from Monte Carlo
282 simulations.

283 Fig. 6 (a) demonstrates that the approximate SPT expression completely fails in
284 describing **this quantity at high pressure**. The main problem with this expression
285 is its incapability to scale correctly from small to large cavity radii. Differently to
286 what has been observed at ambient conditions [10], comparison with simulation
287 results shows a qualitative disagreement. This happens for values of a_w in a quite
288 large range (1.50 – 2.94 Å). Reducing this parameter, the convergence to the
289 asymptotic value of $G(r)$ is as rapid as that observed for simulation results, **even if**
290 **with an incorrect sign of the curve’s slope**. This indicates that a simple reduction
291 **of the value of this parameter is not sufficient to significantly improve the perfor-**
292 **mance of the approximate SPT expression**. However, it would seem reasonable to
293 **presume a value for $\tilde{\gamma}$ which at 8000 atm is lower than that at 1 atm, in contrast**
294 **with what is found if a_w is chosen on the basis of the most probable O-O distance.**
295 **Namely, this is valid within the usual approach for which the excluded volume**
296 **times P is included in μ^* , as in Eq. (2).**

297

298 *3.4.2. Fitting with the simple model at 8000 atm*

299 Working within the framework of the thermodynamics of surfaces (Eq. (2) and
300 Eq. (4)), with the simplest model ($\alpha = 0$) for the cavity surface term, one has to fix
301 the value of two independent parameters, $\tilde{\gamma}$ and $\tilde{\delta}$. These can be determined from
302 the linear fitting of the surface contribution to the derivative of μ^* with respect to
303 r . Linear fitting of data at 8000 atm compared with that at 1 atm shows a generally

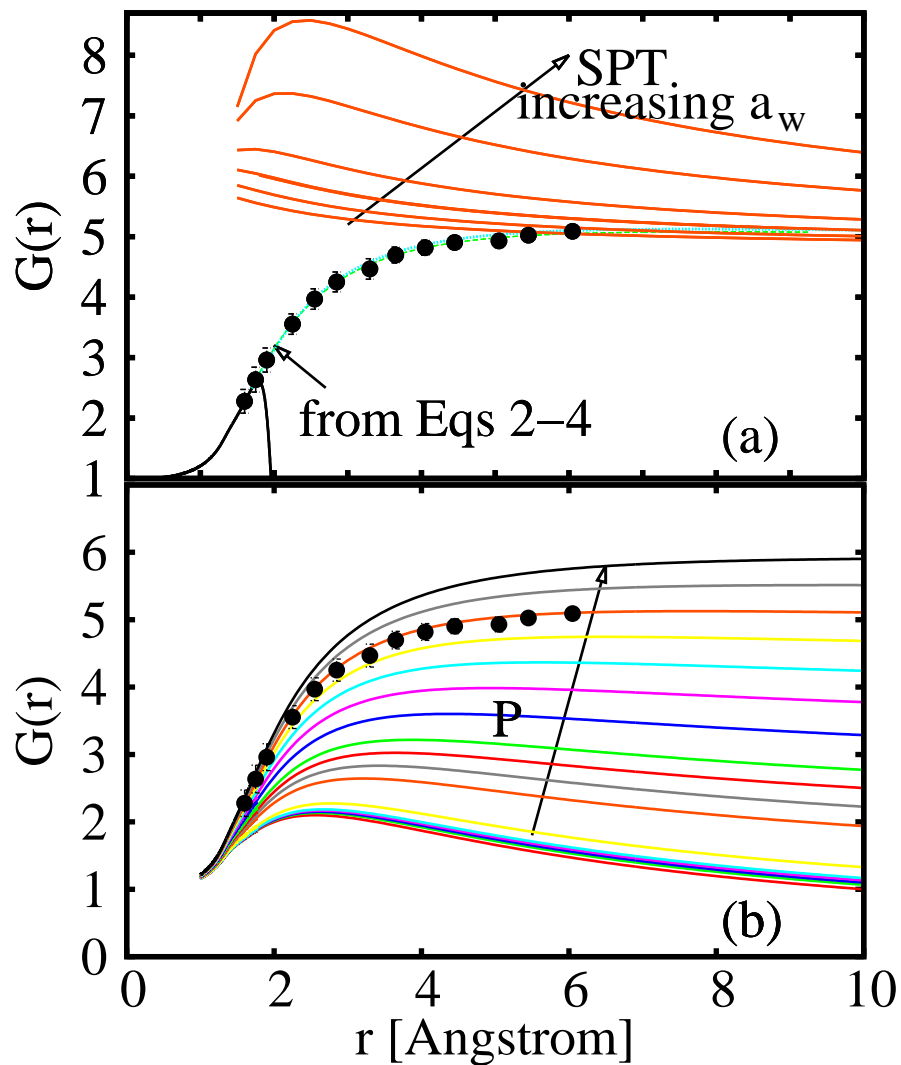


Figure 6: Contact values of the cavity-water oxygen rdFs for cavities in TIP4P water at 298 K. (a) Results at 8000 atm: from MC NPT simulations (circles with error bars); from approximate SPT expression [13, 14, 10] with values for the water diameter parameter (a_w) between 1.5 Å and 2.94 Å (orange lines); from fitting with the simple model, i.e. using Eqs. 2 - 4 as indicated by the arrow (read text); results for small cavities from Eq. 1 (solid black line). (b) Effect of increasing pressure, as indicated by the arrow, over the range from 1 to 10000 atm for $G(r)$ results obtained from Eqs. 3 and 4 using exact SPT conditions. For the parameters dependence on P see Fig. 7. As in (a), circles with error bars are used for MC NPT simulation results at 8000 atm.

304 better performance together with a striking reduction of $\tilde{\gamma}$ and the increase of $\tilde{\delta}$
 305 [10] ($\tilde{\gamma} = 35.4 \text{ dynes/cm}$ and $\tilde{\delta} = 3.8 \text{ \AA}$ when radii less than 2 \AA are not included
 306 in the data). In contrast to the approximate SPT expression, this model gives a
 307 good description of $G(r)$ (Fig. 6 (a)), while the addition of the term depending on
 308 α is necessary to improve the fit if radii less than 2 \AA are included in the data. In
 309 this case $\tilde{\gamma} = 43 \text{ dynes/cm}$, $\tilde{\delta} = 4.1 \text{ \AA}$ and $\alpha = 6.4 \text{ \AA}^3$ were obtained.

310

311 *3.4.3. Using exact SPT conditions to parametrize the simple model along the* 312 *isotherm*

313 Alternatively to fitting, once $\tilde{\gamma}$ is fixed, parameters $\tilde{\delta}$ and α can be obtained by
 314 imposing continuity for $G(r)$ and its derivative at a cavity radius value at the ex-
 315 treme of validity of Eq. (1). Results are shown in Fig. 6 (b) and compared with
 316 simulation results at 8000 atm. By using this procedure, dependence on P of both
 317 parameters is obtained by exploiting Eqs. (7)- (10) for an assumed expression
 318 $\tilde{\gamma}(P)$. Results [presented in Sections 3.4.1 and 3.4.2](#) suggest a decrease in this pa-
 319 rameter with increasing pressure when very far from ambient conditions. In fact,
 320 reasonable agreement with $G(r)$ simulation data at 8000 atm is obtained for $\tilde{\gamma}$ in
 321 the range of 35-48 dynes/cm. [10].

322 **However, despite the failure to predict correct results for radii less than 6 \AA , at**
 323 **large radii the approximate SPT expression** can be used to compute $\tilde{\gamma}(\rho)$. Using
 324 the ρ value from simulations, values of $\tilde{\gamma}$ in the range above were obtained from
 325 the approximate SPT expression for a_w in the range between $2.2\text{-}2.4 \text{ \AA}$. Thus,
 326 it could appear justifiable to fix the high pressure asymptotic value of this pa-
 327 rameter at 2.4 \AA , which is close to the O-O minimum contact distance in water.
 328 Dependence on P of this parameter might be modeled by assuming a transition

329 between the values of the low and high pressure limits. An example is given in
330 Fig. 7 (a)(**blue curve**). We notice that **the corresponding $\tilde{\gamma}$ (P) profile (green**
331 **curve) predicts reasonable values at 1 and 8000 atm where it** shows a positive and
332 negative slope respectively.

333 However, this **approach** can result somewhat arbitrary without some additional
334 information on the pressure at which **the slope sign changes**. For this reason the
335 pressure profile of parameter $\tilde{\gamma}$ was preferred based on simulation results of $G(r)$
336 obtained for the largest cavity studied in this work (6.05 Å). When these values
337 were introduced into the approximate SPT expression, the corresponding a_w were
338 found to be in good agreement up to 8000 atm with the hypotized pressure profile
339 for this parameter **(in Fig. 7 (a) you can compare squares with the blue line)**.

340 **On the contrary**, when using Eq. (3) and Eq. (4), $\tilde{\gamma}$ was varied until $G(r)$ values
341 reached agreement with simulation results. At the same time, parameters $\tilde{\delta}$ and α
342 were determined by the requirement of continuity for $G(r)$ and $G'(r)$ at a cavity
343 radius value of 1.67 Å with the **values obtained from** Eq. (1). This was readily
344 done at any possible value of P by exploiting Eq. (7) and Eq. (9). Fig. 7 shows the
345 pressure dependence for all parameters entering Eq. (4), including w_0 , which was
346 finally fixed by imposing continuity for μ^* . Results confirm that the slope sign for
347 $\tilde{\gamma}$ is positive at 1 atm and negative at 8000 atm, even if the profile in comparison
348 to that obtained from the approximate SPT presents a less pronounced curvature
349 with a different position for the maximum value. Nevertheless, such disagreement
350 is within statistical uncertainties on $\tilde{\gamma}$, which are unfortunately very sensitive to
351 statistical uncertainties on $G(r)$.

352 In contrast to $\tilde{\gamma}$, all the other parameters show a pressure dependence with positive

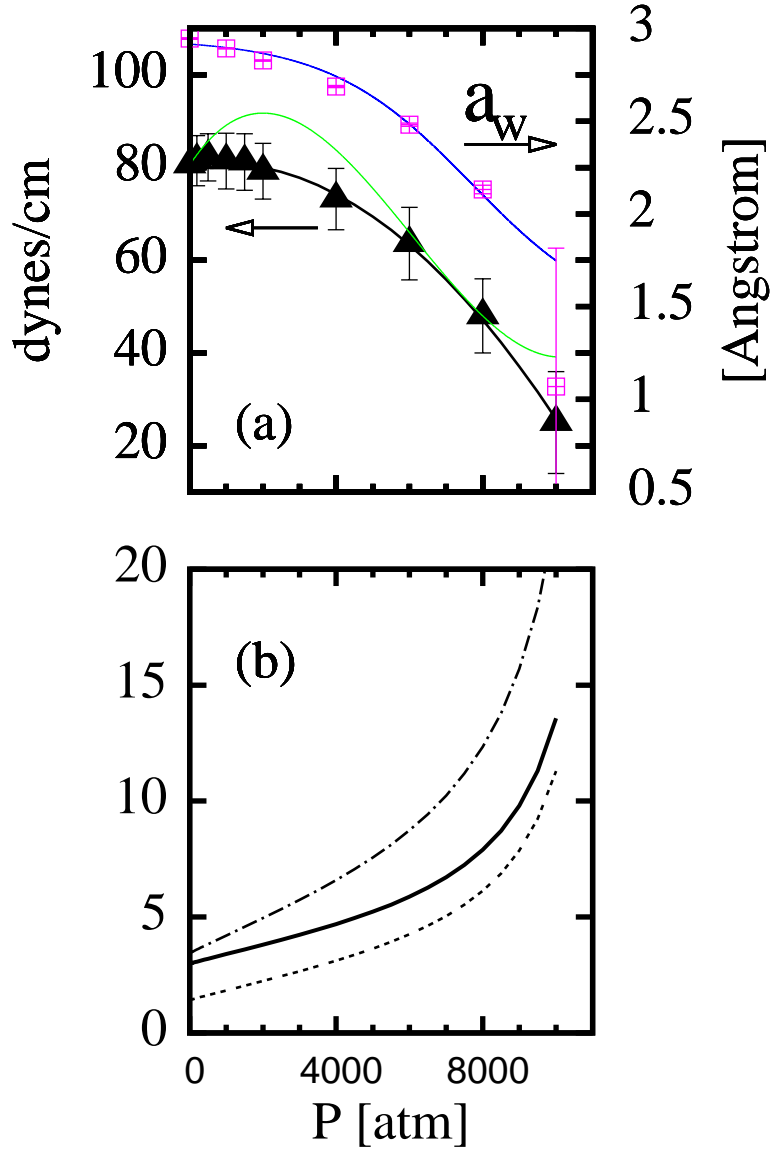


Figure 7: P dependence at T=298 K for parameters entering μ^* computed by using the simple model (Eq. (2)). (a) $\tilde{\gamma}$ obtained from $G(r)$ for $r = 6.05 \text{ \AA}$ (triangles, left scale) fitted by a quadratic function (solid black line). The squares (right scale) are for the corresponding values of SPT parameter a_w . The green line represents $\tilde{\gamma}$ values derived by approximate SPT from $a_w(P)$ described by the blue line (right scale). (b) Parameters entering $f_c(r)$ for $\tilde{\gamma}$ described by the solid black line in (a) : $\tilde{\delta}$ (solid line) in \AA , $\tilde{\alpha}$ (dotted line) in \AA^3 , $w_0/(4\pi\tilde{\gamma})$ (solid dotted dashed line) in \AA^2 (see Eq. (3) of Ref. [10]).

353 slope throughout the examined range with a steep increase at P greater than 8000
354 atm. Such behavior is not of easy interpretation in the absence of a clear physical
355 meaning of these parameters. We merely note that this alternative parametrization
356 leads to values which are in agreement with those obtained by fitting, in particular
357 at 8000 atm. Thus, contact values of cavity-O rdfs at 8000 atm from the radial
358 derivative of μ^* are in agreement with simulation results and fitted values (Fig. 6
359 (a)). In Fig. 6 (b), results from the same equation are shown over the range of P
360 from 1 to 10000 atm.

361 **4. Conclusions**

362 Simulation results of water distribution around a cavity at 8000 atm presented
363 in this work clearly show a very different behavior with respect to 1 atm when
364 increasing the cavity radius. In particular, the concurrent progressive dewetting
365 at the contact distance is peculiar of low pressure conditions, while at very high
366 pressure there is persisting structure.

367 The rdf's contact value, $G(r)$, is confirmed to be a valid quantity in parametrizing
368 and testing heuristic expressions for the excess chemical potential. In contrast to
369 the approximate SPT expression, simple expressions formulated within the ther-
370 modynamic of surfaces are able to catch the main features of cavities in water
371 over a wide range of pressure. However, in this framework there are possible
372 improvements by testing pressure derivatives of the excess chemical potential on
373 excess volumes and excess compressibility. To this aim, the method adopted here
374 to find pressure dependence of parameters appears quite convenient due to the
375 use of pressure dependence of pure water quantities and only limited and easily
376 available information on cavities in water. At least for the expression tested in this

377 work, which adopts the common division of the excess chemical potential in terms
378 of the accessible surface and the exclusion volume, it was found that parameters
379 determined with this method are in agreement with values obtained from normal
380 fitting procedures.

381 **5. Appendix A**

382 We notice that Eq. (9) has been applied to small cavities such that the maximum
383 number of oxygen centers observed in pure water in a sphere of radius r is 2. In
384 this case, the average number of oxygen pairs observed in the same region is the
385 probability of finding exactly 2 centers[3]. Given that this is a rare event, as first
386 approximation one can assume a Poisson distribution [30]

$$P_2 = \frac{\langle n \rangle^2}{2!} \exp[-\langle n \rangle]. \quad (11)$$

387 Thus, Eq. (9) corresponds to a modified Poisson distribution, namely

$$P_2 = \left[\frac{\langle n \rangle^2}{2!} \exp[-\langle n \rangle] \right]^{B(r, \langle n \rangle)} \quad (12)$$

388 where B is a function of the cavity radius and on the solvent density through the
389 average number of oxygen centers in the spherical volume. It was found that,
390 **regardless of the pressure**, the B value is generally greater than 1 when $\langle n \rangle$ is
391 less than 1. For radii at the extreme of the interval for which the maximum value
392 of n is 2, $\langle n \rangle$ is around of 1 and B approaches 1 (Fig. 8 (a)).

393 Therefore, a smaller average number of pairs is observed with respect to the Pois-
394 son distribution for smaller radii. To further examine deviations from the Poisson

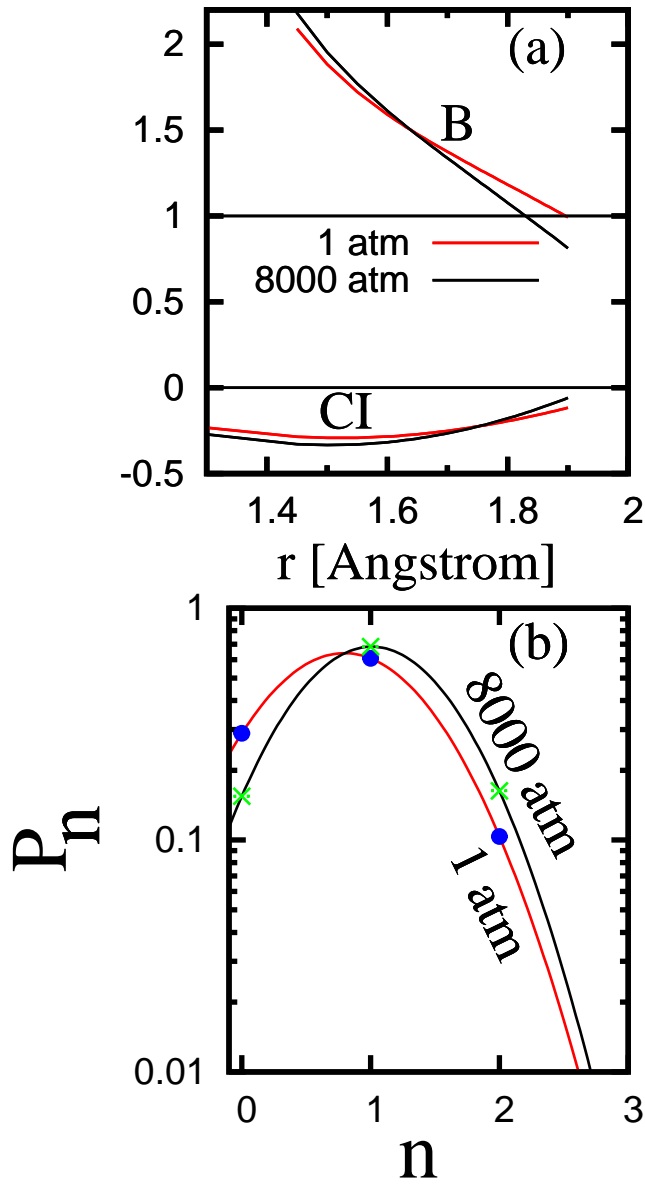


Figure 8: (a) The radial dependence of the exponent B in the modified Poisson distribution (Eq. (12)) and the correlation index CI (Eq. (14)) at 1 atm and 8000 atm. B computed from Eq. 15 in terms of $\langle n \rangle$ using Eq. 7 for ρ . Crossover with horizontal lines indicate cavity radii at which the modified distribution coincides with a Poisson distribution. (b) P_n , the probability to find exactly n water-oxygen in a spherical region. Results refer to a radius of 1.8 Å at 1 atm and 8000 atm. Points indicate simulation results, while the curves come from parabolic fitting of the probability described with the modified Poisson distribution with B from eq. 15.

395 distribution, also the ratio between variance and $\langle n \rangle$ has been taken into ac-
 396 count. This ratio is 1 for the Poisson distribution of a certain, unlimited number
 397 of events. When n can assume a maximum value of 2, only three possible events
 398 can occur, and if also P_1 follows a Poisson distribution, this ratio would be:

$$\frac{\sigma_n^2}{\langle n \rangle} = \frac{\langle n \rangle}{1 + \langle n \rangle} + 1 - \langle n \rangle . \quad (13)$$

399 By assuming that $\langle n \rangle$ is given by Eq. (10) and computing variance from $\langle n \rangle$
 400 and the average number of pairs, the following index was computed:

$$CI = \frac{\sigma_n^2}{\langle n \rangle} - \left(\frac{\sigma_n^2}{\langle n \rangle} \right)_{Poisson} . \quad (14)$$

401 Here the same symbol used for the clustering index introduced for comparison
 402 with the Poisson distribution in studies of drop clustering is adopted. A plot of
 403 CI versus the cavity radius is shown in Fig. 8 (a) for pressures of 1 atm and 8000
 404 atm. It can be noted that CI is zero approaching the radius at the extreme of the
 405 interval for which the maximum value of n is 2. This radius is quite close to that
 406 at which the exponent B in Eq. (12) is 1.

407 In order to compute the pressure derivative of the excess chemical potential, de-
 408 pendence of B on $\langle n \rangle$ was studied at fixed r by looking for a model that at
 409 the same time works well for different cavity radii. In this respect it was also
 410 important that optimized parameters showed continuous dependence on r . For
 411 cavities in which the maximum number of oxygen centers is 2, it was found that
 412 such dependence is reasonably described by the following expression

$$B[r, \langle n \rangle] = b_0(r) + b_1(r) \langle n \rangle + b_2(r) \langle n \rangle^2 + \frac{b_3(r)}{\langle n \rangle} \quad (15)$$

413 where parameters b_0 , b_1 , b_2 and b_3 are functions of r . Also a second-degree poly-
 414 nomial fit was taken into account as it is also able to describe the observed depen-
 415 dence. Nevertheless, Eq. (15) was preferred on the basis of a systematically lower
 416 value of χ^2_ν and generally better behavior of residual observed by comparing the
 417 two models for the same choice of weights.

418 Hence, from a study of the number of pairs against cavity radius at a fixed pres-
 419 sure, parameters entering Eq. (15) can have the general form

$$b_k(r) = \alpha_0 + \sum_{l=1}^{l_1} \alpha_l r^l + \sum_{l=1}^{l_2} \beta_l r^{-l} \quad (16)$$

420 with α_l and β_l independent of density. A strict test of radial dependence of these
 421 functions regards the prediction of **G(r) values by computing the derivative of μ^***
 422 with respect to r . In fact, this implies also a good description of first derivatives
 423 of these functions. A possible radial dependence of b_0 , b_1 , b_2 and b_3 is given by
 424 the following expressions:

$$b_0(r) = \alpha_0 + \alpha_1 r + \alpha_2 r^2 + \frac{\beta_1}{r} + \frac{\beta_2}{r^2} \quad (17)$$

$$b_1(r) = \frac{\beta_1}{r} + \frac{\beta_2}{r^2} + \frac{\beta_3}{r^3} + \frac{\beta_4}{r^4} + \frac{\beta_5}{r^5} \quad (18)$$

$$b_2(r) = \frac{\beta_4}{r^4} + \frac{\beta_5}{r^5} + \frac{\beta_6}{r^6} + \frac{\beta_7}{r^7} + \frac{\beta_8}{r^8} \quad (19)$$

$$b_3(r) = \alpha_1 r + \alpha_2 r^2 + \alpha_3 r^3 + \alpha_4 r^4 + \alpha_5 r^5. \quad (20)$$

425 According to these equations and Eq. (10), radial dependence of B is the same
426 as that of b_0 . Appropriate values of α_l and β_l were found for each coefficient b_k
427 entering Eq. (15) by least squares minimization [27].

428 Finally, for a specific cavity radius at constant pressure, the probability P_n was
429 obtained from Eqs. (9) and Eq. (10) using ρ from Eq. (7) and fitted with the form
430 derived from an information theory based on the first two moments and using a
431 flat default model, namely

$$P_n = \exp[\lambda_0 + \lambda_1 n + \lambda_2 n^2]. \quad (21)$$

432 The curves obtained in this manner for a cavity of 1.8 Å are shown in Fig. 8
433 (b) at 1 and 8000 atm. These curves practically overlap those obtained fitting the
434 simulation results. At 1 atm, our results compare very well with the information
435 theory results obtained by Hummer et al. [12] using another model potential for
436 water.

437 **Supplementary Material**

438 Parameters entering Eqs. 7-9.

439 [1] A. Ben-Naim, Statistical Thermodynamics for Chemists and Biochemists,
440 Plenum, New York, 1992.

441 [2] D. Ben-Amotz, F. O. Raineri, G. Stell, Solvation thermodynamics: Theory
442 and applications., J. Phys. Chem. B 109 (2005) 6866.

443 [3] H. Reiss, H. Frish, J. Lebowitz, Statistical mechanics of rigid spheres, J.
444 Chem. Phys. 31 (1959) 369.

- 445 [4] F. H. Stillinger, Structure in aqueous solutions of nonpolar solutes from the
446 standpoint of scaled-particle theory, *J. Solution Chem.* 141 (1973) 197.
- 447 [5] F. Floris, M. Selmi, A. Tani, J. Tomasi, Free energy and entropy for inserting
448 cavities in water: Comparison of monte carlo simulation and scaled particle
449 theory results, *J. Chem. Phys.* 107 (1997) 6353.
- 450 [6] H. S. Ashbaugh, L. Pratt, Scaled-particle theory and the length scales of
451 hydrophobicity, *Rev. Mod. Phys.* 78 (2006) 159.
- 452 [7] J. Tomasi, B. Mennucci, R. Cammi, Quantum mechanical continuum solva-
453 tion models, *Chem. Rev.* 105 (8) (2005) 2999–3093.
- 454 [8] C. Amovilli, C. Filippi, F. M. Floris, Quantum monte carlo formulation
455 of volume polarization in dielectric continuum theory, *J. Chem. Phys.* 129
456 (2008) 244106.
- 457 [9] C. Amovilli, F. M. Floris, Study of dispersion forces with quantum monte
458 carlo: Toward a continuum model for solvation, *J. Phys. Chem. A.* 5327
459 (2015) 244106.
- 460 [10] F. M. Floris, Modeling the cavitation free energy, *J. Phys. Chem. B* 109
461 (2005) 24061.
- 462 [11] T. L. Hill, *Statistical Mechanics*, Dover Publications, New York, 1956.
- 463 [12] G. Hummer, S. Garde, A. E. Garcia, A. Pohorille, L. R. Pratt, An information
464 theory model of hydrophobic interactions, *Proc. Natl. Acad. Sci. USA* 93
465 (1996) 8951–8955.

- 466 [13] A. Pierotti, A scaled particle theory of aqueous and nonaqueous solutions,
467 Chem. Rev. 76 (1976) 717.
- 468 [14] J. Postma, H. Berendsen, J. Haak, Thermodynamics of cavity formation in
469 water, Faraday Symp. Chem. Soc. 17 (1982) 55.
- 470 [15] J. Rowlinson, B. Widom, Molecular Theory of Capillarity, Clarendon Press,
471 Oxford, 1951.
- 472 [16] L. Pratt, A. Pohorille, Theory of hydrophobicity: Transient cavities in molec-
473 ular liquids, A. Proc. EBSA Workshop on Water-Biomolecular Interactions
474 43 (1992) 261.
- 475 [17] H. S. Ashbaugh, T. M. Truskett, Putting the squeeze on cavities in liq-
476 uids: Quantifying pressure effects on solvation using simulations and scaled-
477 particle theory, J. Chem. Phys. 134 (2011) 014507.
- 478 [18] W. Jorgensen, J. Chandrasekhar, J. Madura, R. Impey, M. Klein, Comparison
479 of simple potential functions for simulating liquid water, J. Chem. Phys. 79
480 (1983) 926.
- 481 [19] W. Jorgensen, BOSS, version 3.5, Yale University Press, New Haven, CT,
482 1994.
- 483 [20] In order to do this we modified the program BOSS [see Ref. 18].
- 484 [21] F. M. Floris, Nonideal effects on the excess volume from small to large cav-
485 ities in tip4p water., J. Phys. Chem. B 108 (2004) 16244.

- 486 [22] A. Kalinichev, Y. Gorbaty, A. Okhulkov, Structure and hydrogen bonding of
487 liquid water at high hydrostatic pressures: Monte carlo npt-ensemble simu-
488 lations up to 10 kbar, *J. Mol. Liq.* 82 (1999) 57.
- 489 [23] M. S. Moghaddam, H. S. Chan, Pressure and temperature dependence of hy-
490 drophobic hydration: Volumetric, compressibility, and thermodynamic sig-
491 natures., *J. Chem. Phys.* 126 (2007) 114507.
- 492 [24] M. W. Mahoney, W. L. Jorgensen, A five-site model for liquid water and
493 the reproduction of the density anomaly by rigid, nonpolarizable potential
494 functions, *J. Chem. Phys.* 112 (2000) 8910.
- 495 [25] H. Sato, M. Uematsu, K. Watanabe, A. Saul, W. Wagner, A fundamental
496 equation for water covering the range from the melting line to 1273 k at
497 pressures up to 25000 mpa, *J. Phys. Chem. Ref. Data* 17 (1988) 1439.
- 498 [26] J. R. MacDonald, Some simple isothermal equations of state, *Rev. Mod.*
499 *Phys.* 38 (1966) 669.
- 500 [27] See Supplemental Material Document No. for parameters entering
501 radial functions $b_0(r)$, $b_1(r)$, $b_2(r)$, $b_3(r)$.
- 502 [28] H. Reiss, E. Helfand, H. Frish, J. Lebowitz, Aspects of the statistical ther-
503 modynamics of real fluids, *J. Chem. Phys.* 32 (1960) 119–124.
- 504 [29] G. Graziano, Scaled particle theory of the length scale dependence of cavity
505 thermodynamics in different liquids, *J. Phys. Chem. B* 110 (2006) 11421–
506 11426.

507 [30] P. Vallery, A. J. Patel, D. Chandler, An improved coarse-grained model of
508 solvation and the hydrophobic effect, *J. Chem. Phys.* 134 (2011) 074109.